Paper 19

12th Symposium on Measuring Techniques
for Transonic and Supersonic Flow in Cascades and Turbomachines

Prague, Czech Republic, September 12-13,1994

FILM COOLING OF AN ANNULAR TURBINE STATOR VISUALISATION OF COOLING AIR EJECTION AND ITS EFFECT ON THE AERODYNAMIC LOSSES

C. Langowski. P. Voigt
Inst. f. Luft und Raumfahrt Koln
Germany

Abstract

Annular turbine cascade tests were carried out to investigate the influence of film cooling on the aerodynamic performance. To obtain detailed information about the secondary flow field and the stator efficiency the flow field downstream of the blade row was investigated using 5-hole-probes at local blowing rates of $0.0 \leq M_l \leq 1.4$. The coolant ejection was visualised by a Laser-Light-Sheet adding oil particles to the coolant. This shows the penetration of the coolant jet and the mixing process with the main flow. Via the determination of jet luminance the coolant concentration downstream of the ejection hole can be quantified. Thus, conclusions about jet mixing and cooling mechanism and, furthermore, the origin of aerodynamic losses are possible. For the experimental conditions used here the kinetic energy loss coefficient was found to be in the range between $4.6\% \leq \zeta_{kin} \leq 7.2\%$.

1 Introduction

To increase the performance of modern gas turbine engines higher turbine inlet temperatures are required. The common blade materials cannot meet the increasing thermal requirements. To protect the stator blades against the hot environment the application of surface film cooling is a very effective method but increases simultaneously the aerodynamic losses. The cooling process is disturbed by the presence of strong endwall secondary flow which interacts with the coolant. Thus, the nearwall flow direction is affected and contributes to enhanced nearwall mixing. Depending on the blowing rate this complex interaction influences the turbine performance.

Modern gas turbines tend to have smaller aspect ratios and hence the various secondary phenomena interact. This emphasizes the importance of investigations of secondary flows and the effect of film cooling on its intensity.

Only a few studies exist about the effect of film cooling on the aerodynamics of secondary flows in a fully annular, low aspect ratio turbine stator. Köllen and Koschel [7] investigated the individual effect of single row coolant ejection at different blade positions to the downstream flow field and cascade losses (blade aspect ratio 0.91). The work of Sieverding, Arts, Dénos and Martelli [9] concentrated on studying the wake mixing process and loss behaviour of trailing edge ejection in transonic conditions. Heat transfer and aerodynamic measurements by Harasgama and Burton [4] showed the effect of secondary flows on film cooling on

the endwalls.
The present study extends the aerodynamic research on subsonic annular, low aspect ratio turbine stator cascades with multiple row coolant ejection. The loss behaviour, secondary flow characteristics and the coolant mixing process, visualised by Laser-Light-Sheet experiments were investigated and specific results are presented.

2 Test facility

The experiments were carried out at the DLR low speed annular turbine test rig with 25 blades. The test cascade is a scaled version (scaling factor 2.348) of a subsonic, low aspect ratio turbine stator with constant hub and tip radii. It is an open loop continuously operating facility with cold air (maximum temperature 315 K, maximum pressure 2.0 bar) and the following main dimensions:

hub diameter, d_H	0.315 m
tip diameter, d_T	0.400 m

The cascade contains 4 film cooled blades enclosing in its middle the test passage. Cooling air is supplied from a separate pressure vessel up to a maximum temperature of 310 K. The experiments were carried out at equal temperatures of cooling air and main flow. Test results of [3, 4, 8] show, that the density ratio has a negligible effect on the film cooling efficiency and the stator aerodynamics. Thus, the influence of the density ratio existing in a real turbine need not be considered. The flow field downstream of the blade row was measured using a 5-hole-probe with 17 radial and 18 circumferential measuring positions. The axial position of the measuring plane and the blade geometry at midspan is shown in Fig.1. The main dimensions are indicated as follows:

number of blades	25
chord length at mid span, C_{MS}	0.0698 m
aspect ratio	0.61
outlet flow angle, $\overline{\alpha_1}$	20.0^o

The positions of the rows for cooling air ejection and the hole geometry are given in Fig.2.
The characteristic data of the operating point for which the measurements were carried out are listed below:

mass flow rate, $\dot{m}_0$	5.315 kg/s
total pressure, p_{t0}	1.6220 bar
total temperature, T_{t0}	307.0 K
inlet flow angle, α_0 (circumf.)	90^o
inlet flow angle, β_0 (radial)	0^o
turbulence level, Tu_0	4.4 %
inlet Mach number, Ma_0	0.1745
outlet Mach number, $\overline{Ma_1}$	0.6780
Reynolds number, Re	1×10^6
coolant temperature, T_{tc}	307.0 K
local blowing rate, $M_l = \frac{(\rho v)_c}{(\rho v)_{\infty,l}}$	0.0/0.5/1.0/1.4

The results of 5-hole-probe measurements upstream prove, that the inlet flow angle at measuring plane 0 (MP 0) is uniform [10].

3 Measurement technique

3.1 Laser-Light-Sheet Imaging

The aim of the quantitative Laser-Light-Sheet imaging technique is to quantify concentrations in mixing flows. Therefore one fluid component has to be seeded with small particles.
The underlying Lorenz– Mie theory claims that the elastically scattered light is proportional to the number of particles in the probe volume and hence proportional to the concentration of the seeded flow. In the experiments propanediol oil was vapourized and injected into the flow. A monodisperse particle size distribution was not always obtained, probably due to condensation effects within the ducts, but the deviation was small enough to assure a sufficient accuracy.

3.1.1 Light-Sheet Probe

A newly developed Laser-Light-Sheet probe permitted a Light-Sheet to be created inside a turbomachine against the flow direction without affecting the flow field but with the need of protecting the optics.
This protection was realized by blowing air out of a small duct shown in Fig.4.
The light source was an argon ion laser with an average power of 3.5 W, working in multiline mode. The light was coupled into a monomode fiber with a core diameter of 4 μm and a numerical aperture of 0.076. The other end of the fiber was coupled into the probe. The working distance b_2 could be adjusted by varying the distance a between the fiber end and the imaging lens, in the beam path, Fig.3. In the test facility a working distance of $b_2 = 150$ mm was used. With the given imaging properties this

yielded a Light-Sheet thickness of 700 μm in the beam waist.
The Light-Sheet generation usually requires an imaging system with at least one spherical and one cylindrical lens. In contrast the new probe created the Light-Sheet with only one rod lens where the fiber aperture replaced the spherical lens resulting in a small overall size.

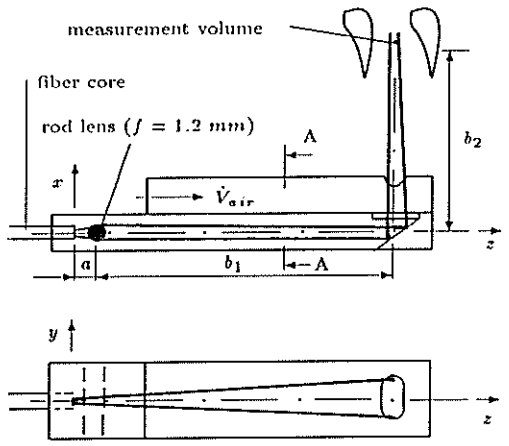

Figure 3: Imaging device with beam path

The imaging device was mounted inside a tube in order to provide the air circuitry.

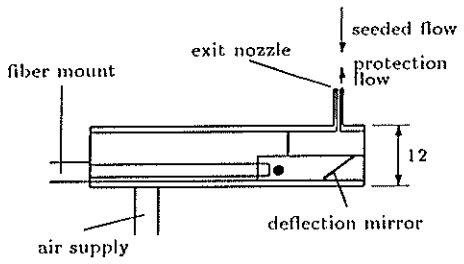

Figure 4: Light-Sheet-Probe, inside mount

The air was blown out at a speed that inhibited the seeded flow to enter the probe through the nozzle and to damage the deflection mirror. The protecting air as well as the Light-Sheet left the probe through the rectangular exit nozzle. To protect the imaging device against mechanical damage it was fixed inside a mount (Fig.4) that could be installed inside the turbomachine like a common probe.
The outer diameter of the mount was 12 mm and thus did not influence the main flow. The scheme of the Light-Sheet technique and the probe installation inside the experimental station is shown in Fig.5.

3.1.2 Image Processing

The Laser-Light-Sheet was imaged onto a CCD-camera (Panasonic VC 1960) with 800 x 600 light sensitive elements. The resulting signal was digitized using an 8 bit frame grabber with a resolution of 768 x 576 pixels.
The reflected light from the blade surface could be partially eliminated by subtracting the so called *lightfield* images from the *specimen* images. The latter were produced with the presence of Light-Sheet and seeding particles whereas in the *lightfield* mode the particle supply is suppressed.
For the evaluation the resulting gray levels were transformed to relative concentrations, with the concentration at the exit of the cooling hole set to 100 percent. Gray level intervals could then be interpreted as regions of equal concentration. For a better representation pseudo-colors were assigned to gray levels.

3.2 5-hole-probe

The used 5-hole-probe is moveable in the radial direction. Pitchwise traversing was achieved by turning the complete stator hub with the blades. Thus, a tip leakage exists of about 0.03 mm. The probe is fixed at the average outlet flow angle $\overline{\alpha_1}$. This reduces the measuring time, because there is no necessity to align the probe with the local flow direction at each measurement point. For this application the 5 -hole -probe has to be calibrated three - dimensionally (two flow directions α, β and Mach number). Polynomial approximations are used to relate the data of calibration with the measurement data.

4 Results and discussion

The coolant ejection behaviour was investigated as an example at mid span of cooling row No. 3. Fig.6 shows an original video shot of the coolant jet development on the blade surface. Because of instationary effects 20 shots were averaged for each blowing rate, digitized and subsequently pseudo-colored. The resultant pictures are shown in Fig.7.
As the temperatures of the cooling air and the main flow are the same, the densities are almost equal. Consequently the blowing rate represents the velocity ratio between the two fluid streams.

For the local blowing rate of $M_l = 0.5$ the jet penetrates into the boundary layer to approximately half of its extension and thickens it. The cooling air always remains on the blade surface, thus, the interaction with the main flow only takes place on the outside of the jet. Since the jet behaves like an obstacle in a stream the lower part of the profile boundary layer in front of it rolls up into the horse-shoe vortex. Only a slight difference of velocity may exist on the outside of the jet between the coolant and the upper part of the boundary layer. Therefore small shear stresses decrease the turbulent mixing process and the dissipation. Hence a high level of cooling air concentration is kept on the blade surface for a long distance and a good cooling efficiency is guaranteed.
Increasing the local blowing rate to $M_l = 1.0$ the jet lifts off from the blade surface, reaches the border of the boundary layer and reattaches after 7 hole diameters downstream with lower concentration. Because of the vortex structure of each single coolant jet material from the main flow and the boundary layer is absorbed. Behind the jet the wake vortex interacts with the legs of the horse-shoe vortex. These turbulent processes are very diffusive and, because of the high Reynolds number very fast ($t_{turb} \sim \frac{1}{Re} t_{mol}$ for turbulent transport processes, [13]). In conclusion it can be seen that the coolant concentration decreases quickly and after reattaching, the cooling efficiency is strongly weakened. Inside the inclined hole the jet is pushed to the outer wall of the bore by a separation bubble at the sharp inlet edge. The deflection is clearly perceptible immediately at the hole exit. This supposition is also proven by numerical analysis of this special flow situation.
For the highest blowing rate ($M_l = 1.4$) the jet lifts off at once, pushes through the boundary layer and penetrates deeper into the main flow. There are similar interactions as described above but higher potential differences transport energy and material more rapidly and entails a stronger mixing and dissipation. In consequence the jet is completely mixed after a short distance in an upper region away from the wall with low surface cooling.

Measurements of the flow field downstream show the effects of different blowing rates and the connected coolant ejection behaviour (Fig.8). The location of vortices as well as their orientation can be identified by parallel running isoclinics of the flow angle α and β, respectively, according to a theory of Binder [2]. Thus, the passage vortex at the casing and the two trailing edge vortices can be identified. Due to the radial pressure gradient the hub passage vortex is pressed to the hub. Because of the required spacing between the 5-hole-probe and the hub it was not possible to detect it with this measurement technique. Detailed Laser-Two-Focus measurements will clarify its position. With increased local blowing rates M_l the vortices are shifted clearly outwards, to the hub and the tip. They are forced by the higher momentum cooling air jets. This tendency is also valid for $M_l = 1.0$ and hence not shown in Fig.8.
The distribution of the total pressure ratio shows a region of high loss resulting from the tip leakage flow. The wakes are shaped typically by the secondary vortices. Corresponding to its character the passage vortex only transports low energy boundary layer material but does not produce much loss of energy itself [10]. Therefore the minimum of total pressure does not always agree with the location of the passage vortex. The trailing edge vortex near the hub is very extended. It absorbs material from the blade boundary layer which is drifted down by the radial pressure gradient. For the local blowing rate $M_l = 0.5$ the wake is thickened and the level of the total pressure minimum is lower. This results from the fact that the coolant jets add energy which is smaller than this of the main flow. The wake for $M_l = 1.4$ is weakened, since the level of the coolant energy is higher.
Very important is the aerodynamic performance of a film cooling configuration. It is insufficient to judge the energy transformation with the commonly used total pressure loss coefficient, defined as:

$$\omega = \frac{p_{t0} - \overline{p_{t1}}}{p_{t0} - \overline{p_{st1}}},$$

since the energy of the cooling air is not considered. Its influence can be taken into account by a corrected inlet total pressure p^*_{t0} as below [12]:

$$\omega^* = \frac{p^*_{t0} - \overline{p_{t1}}}{p^*_{t0} - \overline{p_{st1}}}, \quad p^*_{t0} = \frac{\dot{m}_0}{\dot{m}_0 + \dot{m}_c} p_{t0} + \frac{\dot{m}_c}{\dot{m}_0 + \dot{m}_c} p_{tc,ex}$$

The losses of kinetic energy are calculated by the coefficient $\zeta_{kin,ex}$ as:

$$\zeta_{kin,ex} = 1 - \frac{\left(1 - \left(\frac{\overline{p_{st2}}}{p_{t2}}\right)^{\frac{\kappa-1}{\kappa}}\right)\left(1 + \frac{\dot{m}_c}{\dot{m}_0}\frac{c_{p,c}}{c_{p,0}}\frac{T_{tc}}{T_{t0}}\right)}{\left(1 - \left(\frac{\overline{p_{st2}}}{p_{t0}}\right)^{\frac{\kappa-1}{\kappa}}\right) + \sum_{i=1}^{n} \frac{\dot{m}_{c,i}}{\dot{m}_0}\frac{c_{p,c,i}}{c_{p0}}\frac{T_{tc,i}}{T_{t0}}\left(1 - \left(\frac{\overline{p_{st2}}}{p_{tc,ex,i}}\right)^{\frac{\kappa-1}{\kappa}}\right)}.$$

To also take into account the losses arising in the blowing holes the total pressure in the cooling chamber p_{tc} has to be used instead of $p_{tc,ex}$. The averaged values were determinated as follows:

$\overline{p_t}$ mass averaged
$\overline{p_{st}}$ area averaged .

In Fig.9 the total pressure loss coefficient ω^* and the kinetic energy loss coefficient $\zeta_{kin,ex}$ are plotted for different blowing rates. A minimum of losses exists for $M_l = 0.5$. Since the boundary layer is energized by the blowing rates above $M_l \sim 0.3$ [11] and an almost loss-free mixing of the coolant occurs this tendency can be explained. Because of the increase in fluid interaction as discussed before the mixing losses rise rapidly for $M_l \geq 1.0$. The same tendency for the loss production was found by Wilfert [11].
The level of losses produced in the blowing holes is shown in Fig.10. There is a higher loss of kinetic energy up to 1.3 % mainly caused by the previously mentioned separation bubble at the sharp hole inlet. Consequently the inlet geometry should be rounded to avoid this supplementary losses. Another remarkable effect is the increase of the losses only by the presence of the blowing holes. They induce an earlier transition from laminar to turbulent boundary layer. The same order of magnitude for the kinetic loss of energy of about 1.2 % results from investigations by Kiock [6].
Fig.11 presents the radial distribution of the loss of kinetic energy. The highest level is present on the tip where the tip leakage flow disturbs the main flow. A big part of the produced losses originates from the trailing edge vortex. A special effect occurs for $M_l = 1.4$ in 65 - 80 % of the span. The losses increase drastically caused by the stronger interaction of the passage vortex shifted to the tip (see Fig.8) and the tip leakage flow. The effect is very significant since a higher blade loading on the tip occurs. An enlarged loss area also appears in the total pressure ratio distribution.

5 Conclusions

- A newly developed Light-Sheet-Probe enables visualisation of coolant jet ejection and allows precise insights into the mixing process.
- From the aerodynamic point of view $M_l = 0.5$ is the optimum blowing rate. A multitude of experimental heat transfer investigations [1, 5] confirm $M_l = 0.5$ to be the most effective for film cooling.
- A strong interaction between the coolant and the main flow rapidly reduce the concentration of the cooling air jet for $M_l \geq 1.0$.
- There exists a long uncooled blade surface area for $M_l = 1.0$ and a low surface cooling for $M_l = 1.4$ because of the lift off of the coolant jet.
- The secondary vortices are forced away to the hub and the tip for high blowing rates $M_l \geq 1.0$. This induces a stronger, more loss producing interaction with the tip leakage flow.
- The loss of energy produced in the blowing holes increases rapidly for $M_l \geq 1.0$ because of a separation bubble at the sharp edge of the inclined hole inlet.

Acknowledgements

The financial support of AG-Turbo, Germany to this project is gratefully acknowledged. The authors wish to express their gratitude to Mr. M.Beversdorff for his support in development of the measurement technique, Mr. W. Karnatschke and Mr. W. Seelig for their contribution to the executed measurements.

Nomenclature

C	[m]	chord length
d	[m]	diameter
h	[m]	blade height
$\dot{m}$	$[\frac{kg}{s}]$	mass flow rate
M		blowing rate, $M=\frac{(\rho v)_c}{(\rho v)_0}$
Ma		Mach number
N		number of blades
p	[bar]	pressure
r	[m]	radius
Re		Reynolds number, $Re=\frac{\overline{v_1}*C_{MS}}{\nu}$
T	[K]	temperature
t	[s]	time
Tu	[%]	turbulence level
v	$[\frac{m}{s}]$	velocity
x,y,z		cartesian coordinates

α	$[^o]$	circumferential flow angle
β	$[^o]$	radial flow angle
δ	$[m]$	boundary layer thickness
ζ		kinetic energy loss coefficient
ω		total pressure loss coefficient
ν	$[\frac{m^2}{s}]$	kinematic viscosity

Subscripts and Superscripts

0	upstream condition
1	downstream condition
ax	axial direction
c	cooling air
ex	cooling hole exit
H	hub
kin	kinetic
l	local
mol	molecular
MS	mid span
st	static condition
t	total condition
turb	turbulent
T	tip
–	averaged
*	corrected

Symbols

MP	measuring plane
PS	pressure side
SS	suction side

References

[1] Bergeles, G.; Gosman, A. D.; Launder, B. E.
Near-field character of a jet discharged through a wall at 30° to a mainstream
AIAA Journal, Vol. 15, No. 4 (1977)

[2] Binder, A.; Romey, R.
Secondary flow effects and mixing of the wake behind a turbine stator
ASME 82-GT-46 (1982)

[3] Haller B.R.; Camus, J.-J.
Aerodynamic loss penalty produced by film cooling transonic turbine blades
ASME 83-GT-77 (1983)

[4] Harasgama S.P.; Burton, C.D.
Film cooling research on the endwall of a turbine nozzle guide vane in a short duration annular cascade
Part 1: Experimental technique and results
ASME 91-GT-252 (1991)

[5] Jubran B.; Brown, A.
Film cooling from two rows of holes inclined in the streamwise and spanwise direction
ASME 84-GT-286 (1984)

[6] Kiock, R.
Experimentelle Untersuchungen über den aerodynamischen Einfluß des Ausblasens auf die Strömung durch zwei stark umlenkende Gasturbinengitter
IB 151 - 77/2 Inst. f. Aerodynamik, DFVLR, Braunschweig (1977)

[7] Köllen, O.; Koschel, W.
Effect of film cooling on the aerodynamic performance of a turbine cascade
AGARD-CP-390 (1985)

[8] Launder, B.E.; York, J.
Discrete-hole cooling in the presence of free stream turbulence and strong favourable pressure gradient
Int. J. of Heat and Mass Transfer, Vol.17(1974), pp.1403-1409

[9] Sieverding, C.H.; Arts T.; Dénos R.; Martelli,F.
Investigation of the flow field downstream of a turbine trailing edge cooled nozzle guide vane
ASME 94-GT-209 (1994)

[10] Wegener, D.
Comparison between two 3D-NS-Codes and experiments on a turbine stator
AIAA 92-3042 (1992)

[11] Wilfert, G.
Mischungsvorgänge zwischen Kühlfilmen und Grenzschichten fortschrittlicher Turbinenbeschaufelungen (Kühlluftausblasung bei x/l=0.4)
IB LRT-WE12-93/10, Inst. f. Strahlantriebe, Universität der Bundeswehr München (1993)

[12] Wilfert, G.
The aerodynamic mixing effect of discrete cooling jets with mainstream flow on a highly loaded turbine blade
ASME 94-GT-235 (1994)

[13] Tennekes, H.; Lumley, J. L.
A first course in turbulence
MIT Press, USA (1974)

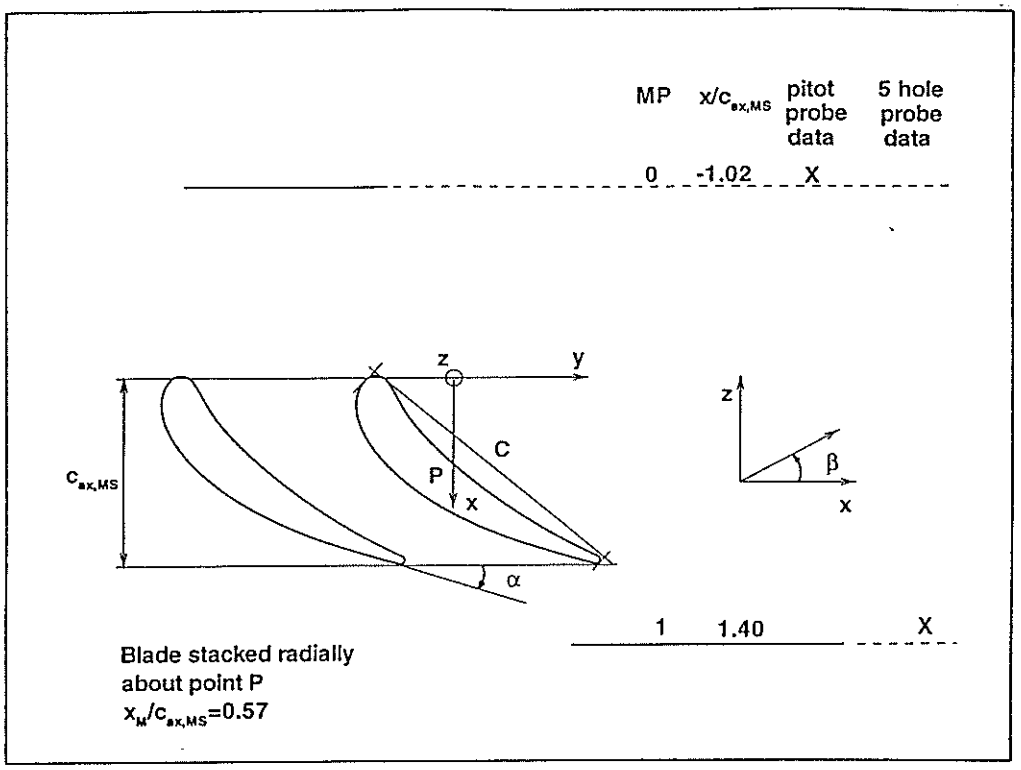

Figure 1: Cascade geometry at mid span and measurement planes

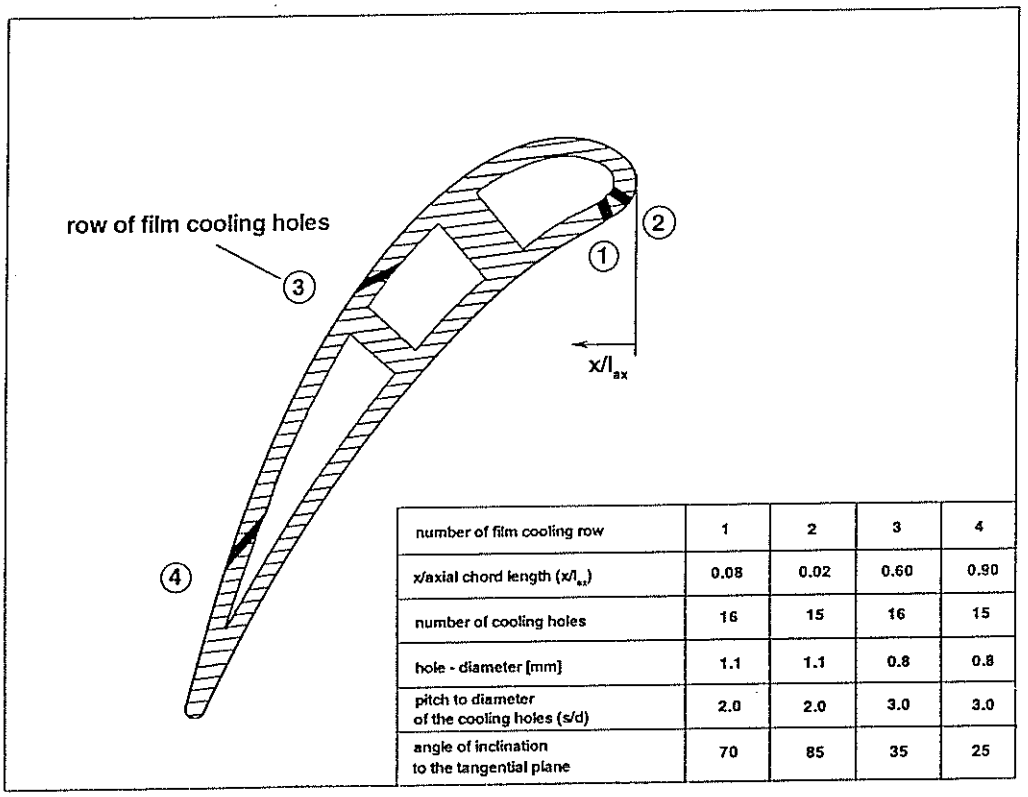

number of film cooling row	1	2	3	4
x/axial chord length (x/l ax)	0.08	0.02	0.60	0.90
number of cooling holes	16	15	16	15
hole - diameter [mm]	1.1	1.1	0.8	0.8
pitch to diameter of the cooling holes (s/d)	2.0	2.0	3.0	3.0
angle of inclination to the tangential plane	70	85	35	25

Figure 2: Arrangement of film cooling rows

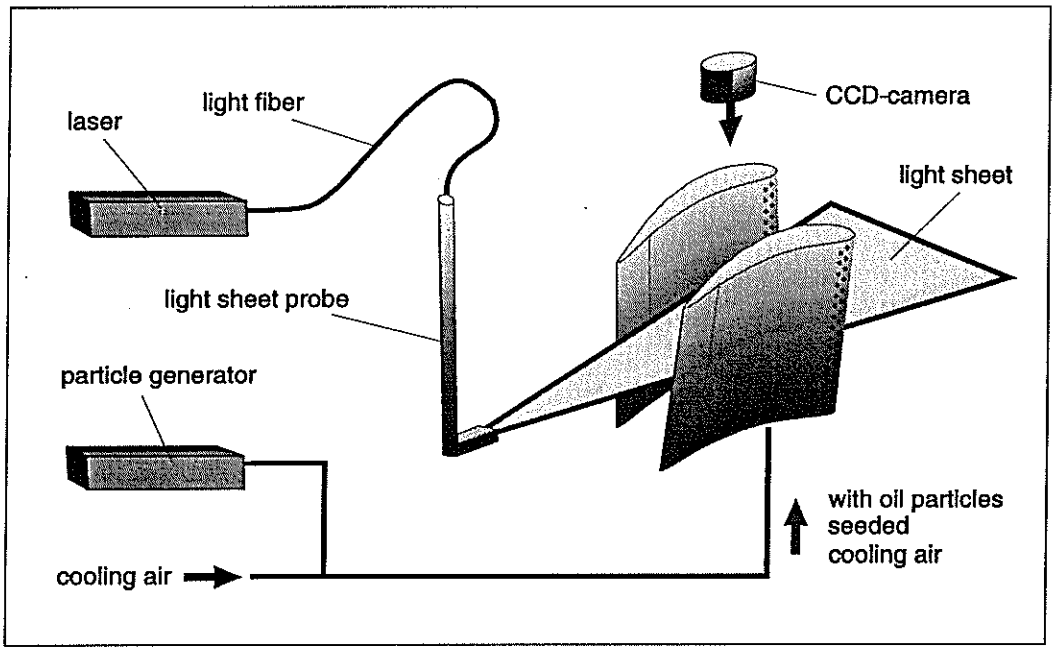

Figure 5: Schematic sketch of visualisation technique

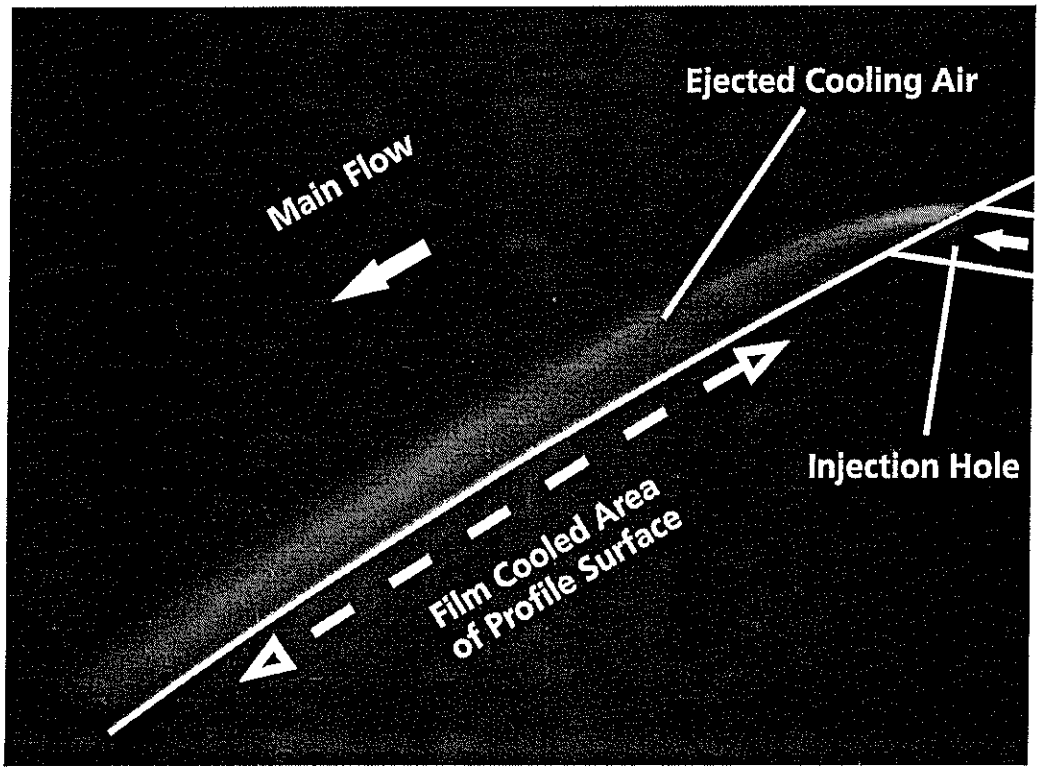

Figure 6: Original video shot of cooling air ejection

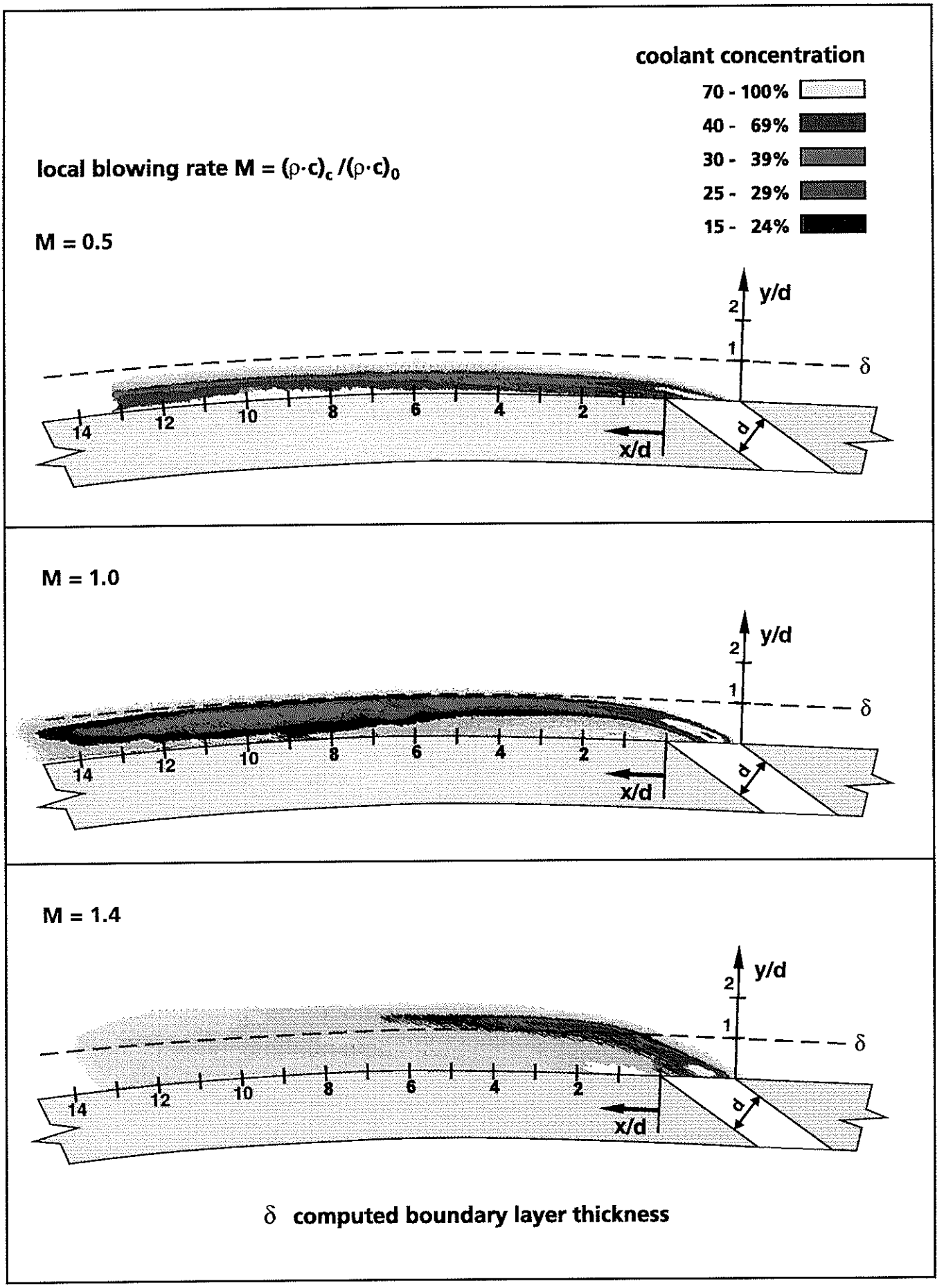

Figure 7: Distribution of cooling air concentration for different blowing rates by pseudo-colored video shots (suction side ejection at row 3, x/l = 0.6)

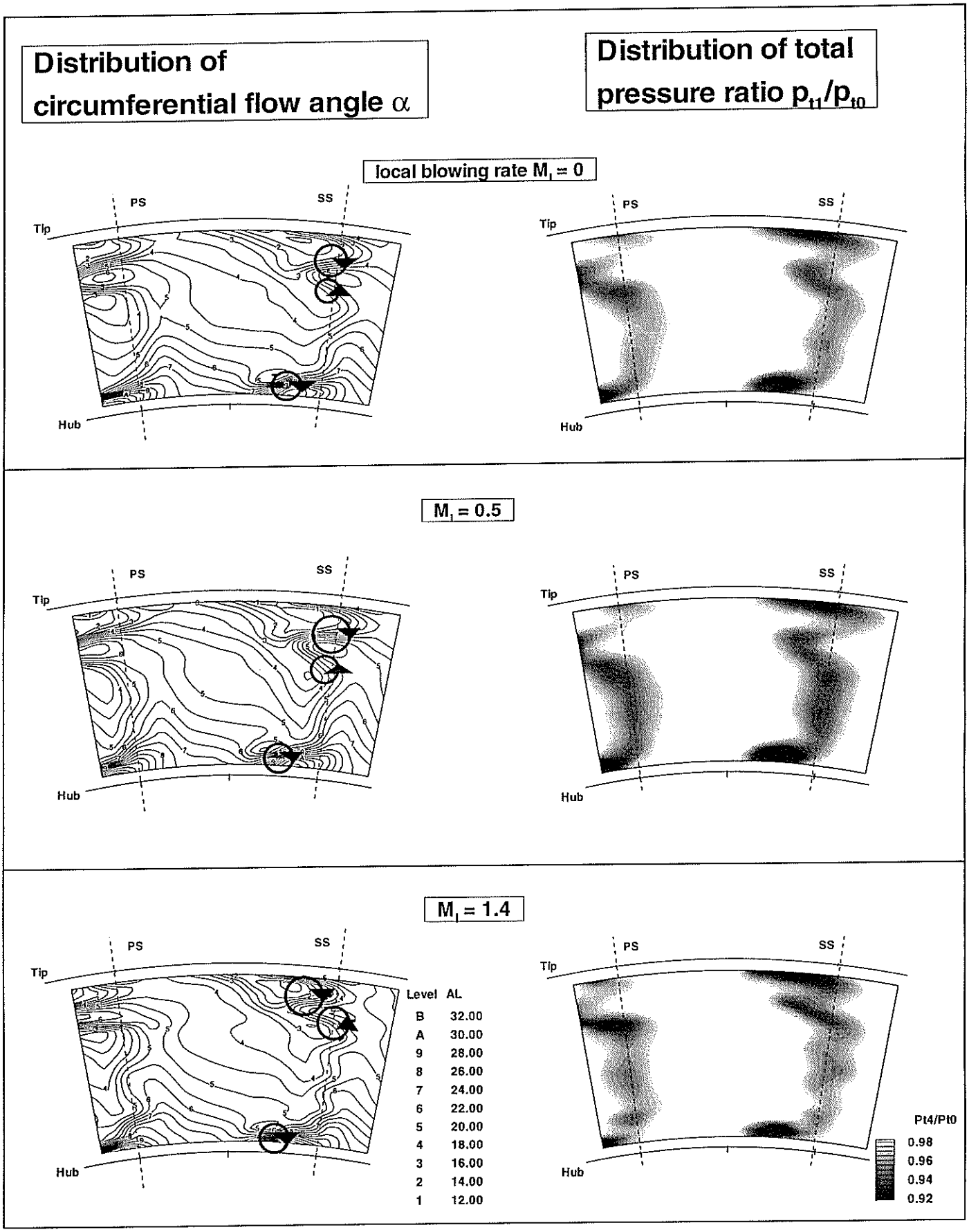

Figure 8: 5-hole probe measurements of the flow field in MP1

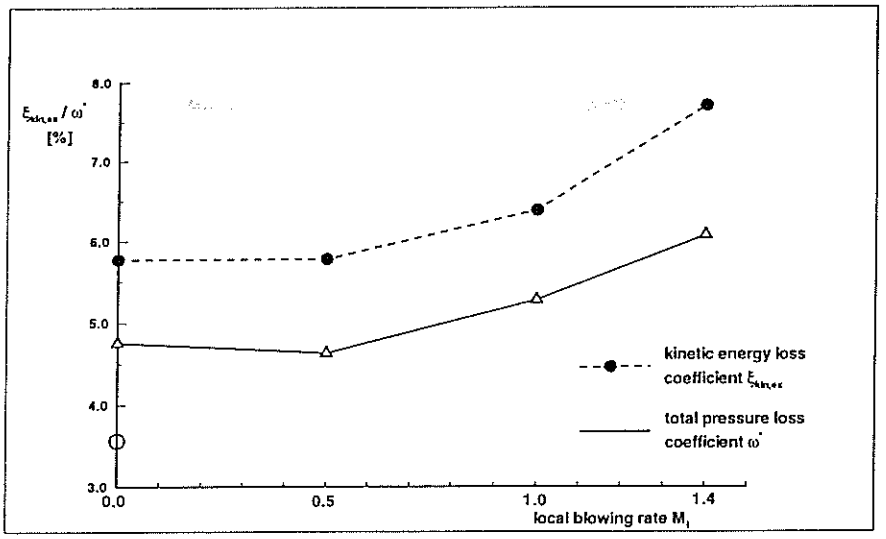

Figure 9: Total pressure loss coefficient ω^* and kinetic energy loss coefficient $\zeta_{kin,ex}$ for different blowing rates

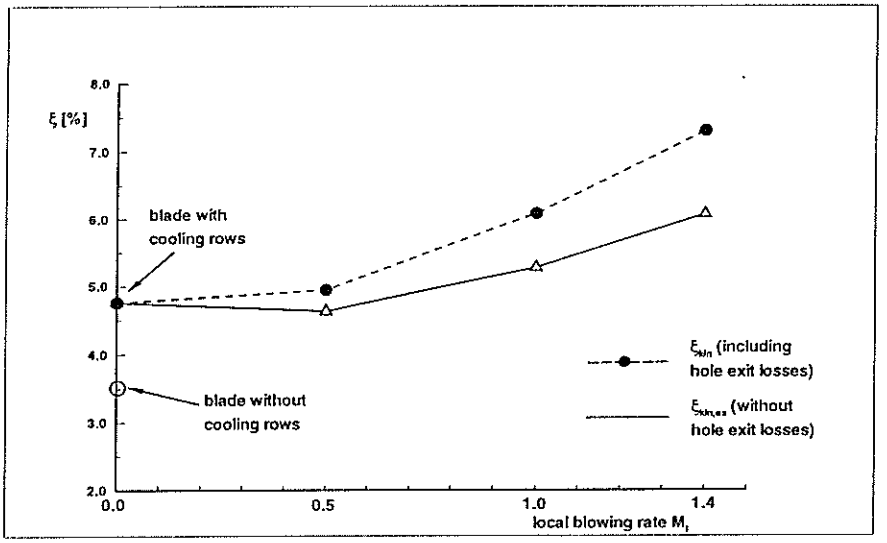

Figure 10: Production of loss of kinetic energy in the blowing holes

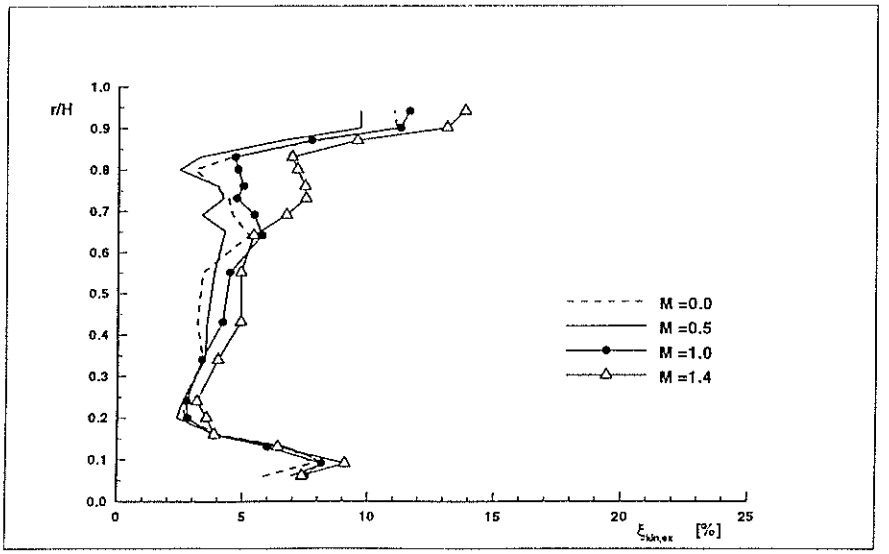

Figure 11: Radial distribution of the kinetic energy loss coefficient $\zeta_{kin,ex}$